An RF-Source-Free Reconfigurable Microwave Photonic Radar With High-Resolution and Fast Detection Capability

Pei Zhou, *Member, IEEE*, Renheng Zhang, Nianqiang Li, *Member, IEEE*, Zhidong Jiang, and Shilong Pan, *Senior Member, IEEE*

***Abstract*—This paper presents a novel microwave photonic (MWP) radar scheme that is capable of optically generating and processing broadband linear frequency-modulated (LFM) microwave signals without using any radio-frequency (RF) sources. In the transmitter, a broadband LFM microwave signal is generated by controlling the period-one (P1) oscillation of an optically injected semiconductor laser. After targets reflection, photonic de-chirping is implemented based on a dual-drive Mach-Zehnder modulator (DMZM), which is followed by a low-speed analog-to-digital converter (ADC) and digital signal processer (DSP) to reconstruct target information. Without the limitations of external RF sources, the proposed radar has an ultra-flexible tunability, and the main operating parameters are adjustable, including the central frequency, bandwidth, frequency band, and temporal period. In the experiment, a fully photonics-based radar with a bandwidth of 4 GHz is established for high-resolution and fast detection. The results show that a high range resolution reaching ∼1.88 cm, and a two-dimensional (2D) imaging resolution as high as ∼1.88 cm × ∼2.00 cm is achieved with a sampling rate of 100 MSa/s in the receiver. The flexible tunability of the radar is also experimentally demonstrated. The proposed radar scheme features low cost, simple structure, and high reconfigurability, which may pave the way for future multifunction adaptive and miniaturized radars.**

***Index Terms*—Microwave photonics, optical injection, radar, semiconductor laser.**

I. Introduction

COMPARED with optical sensors, e.g., lidars, radars are more attractive in terms of the all-time and all-weather operation capability [1]. Fast, high-resolution detection and imaging of objects by radar is highly desired in many emerging applications, such as unmanned aerial vehicles (UAVs) and autonomous vehicles. In order to achieve high-speed and high-resolution target detection, a radio-frequency (RF) radar is required to afford both a broadband transmit signal and a fast signal processing ability [2]. In conventional electrical radars, the transmit signal generated by purely electrical techniques suffers from limited frequency and bandwidth. Although the bandwidth can be promoted through multiple stages of frequency conversion, the performance of the transmit signal in the transmitter as well as the analog-to-digital converters (ADCs) in the receiver would deteriorate rapidly with the increase of the operating bandwidth. Therefore, the resolution and processing speed of the radar are restricted. To cope with these problems associated with electrical methods, numerous microwave photonic (MWP) radar schemes have been proposed [3], [4]. In 2014, P. Ghelfi *et al.* demonstrated the first MWP radar, in which a mode-locked laser is employed to realize the signal generation in the transmitter as well as the optical sampling in the receiver [5]. However, its operating bandwidth and ranging resolution are restricted by the small pulse-repetition frequency. Consequently, different types of broadband linear frequency-modulated (LFM) signal generators have been utilized in MWP radars, including optical wavelength-to-frequency mapping, photonic digital-to-analog convertor, microwave photonic frequency multiplication, and so on [6]–[8]. Among these schemes to realize broadband MWP radars, the majority are based on microwave photonic frequency multiplication for broadband signal generation in the transmitter, and microwave photonic frequency mixing for broadband photonic de-chirping in the receiver [8]–[12]. Thanks to the bandwidth compression property brought by broadband photonic de-chirping, fast and even real-time radar signal processing is

Manuscript received August 24, 2021; revised November 20, 2021 and December 24, 2021; accepted January 11, 2022. Date of publication January 13, 2022; date of current version May 2, 2022. This work was supported in part by the National Natural Science Foundation of China under Grants 62001317, 62171305, and 62004135, in part by the National Key R&D Program of China under Grant 2018YFB2201803, in part by the Natural Science Foundation of Jiangsu Province under Grant BK20200855, in part by the Natural Science Research Project of Jiangsu Higher Education Institutions of China under Grants 20KJB510011 and 20KJA416001, in part by the Open Fund of State Key Laboratory of Information Photonics and Optical Communications (Beijing University of Posts and Telecommunications), China, under Grant IPOC2020A012, in part by the State Key Laboratory of Advanced Optical Communication Systems Networks, China, under Grant 2021GZKF003, and in part by the Project of Key Laboratory of Radar Imaging and Microwave Photonics (Nanjing University of Aeronautics and Astronautics), Ministry of Education, under Grant RIMP2020001. *(Corresponding authors: Nianqiang Li; Shilong Pan.)*

Pei Zhou, Renheng Zhang, Nianqiang Li, and Zhidong Jiang are with the School of Optoelectronic Science and Engineering, Soochow University, Suzhou 215006, China, and with the Key Lab of Advanced Optical Manufacturing Technologies of Jiangsu Province and the Key Lab of Modern Optical Technologies of Education Ministry of China, Soochow University, Suzhou 215006, China. Pei Zhou is also with the Key Laboratory of Radar Imaging and Microwave Photonics, Ministry of Education, Nanjing University of Aeronautics and Astronautics, Nanjing 210016, China (e-mail: peizhou@suda.edu.cn; 20195239032@stu.suda.edu.cn; nli@suda.edu.cn; 20205239013@stu.suda.edu.cn).

Shilong Pan is with the Key Laboratory of Radar Imaging and Microwave Photonics, Ministry of Education, Nanjing University of Aeronautics and Astronautics, Nanjing 210016, China (e-mail: pans@nuaa.edu.cn).

Color versions of one or more figures in this article are available at https://doi.org/10.1109/JLT.2022.3142992.

Digital Object Identifier 10.1109/JLT.2022.3142992

possible. In 2017, a real-time and high-resolution MWP imaging radar was reported with an instantaneous bandwidth of 8 GHz and a two-dimensional (2D) imaging resolution of 2 cm × 2 cm [9]. After that, multiple-input-multiple-output (MIMO), multiband, and phased-array MWP radars were also successfully demonstrated [13]–[18]. However, an intermediate-frequency linear frequency-modulated (IF-LFM) signal is required for those MWP radars based on photonic frequency multiplying. For example, in [12], an IF-LFM signal centered at 11 GHz with a bandwidth of 4 GHz was adopted for photonic frequency doubling, which inevitably increases the complexity and cost of the system. Besides, the electrical IF-LFM signal usually operates efficiently only in a pre-designed frequency band with a specific bandwidth, which would restrain the reconfigurable capabilities of radars. Therefore, an MWP radar that eliminates the limitations of the external RF sources, namely an RF-source-free MWP radar, is highly preferred. Nonetheless, the study of RF-source-free MWP radar has rarely been reported. Recently, X. Zhang *et al.* have demonstrated an RF-source-free MWP radar based on a frequency-sweeping optoelectronic oscillator [19]. The main drawback is the limited linearity of the generated LFM signal in the transmitter, which would lead to poor performance of the photonic de-chirping processing in the receiver. As a consequence, complicated compensation processing is necessary to obtain target information, which definitely slows down the processing accuracy and speed of the radar.

In recent years, a novel approach to generating microwave signals based on an optically injected semiconductor laser (OISL) has been proposed and received increasing attention. By taking advantage of the period-one (P1) dynamics of an OISL, photonic microwave generation with a tunable frequency from a few to over 100 GHz has been achieved without the requirement of any external RF sources [20]–[25]. In addition to tunable microwave signals, P1 oscillations of an OISL have also been applied for generating microwave frequency combs, optical frequency combs, optical pulses, and triangular pulses [26]–[30]. In our prior work, we proposed and experimentally demonstrated the photonic generation of broadband LFM signals by dynamically controlling the injection parameters of an OISL [31]. Furthermore, photonic generation of other useful radar waveforms has also been reported based on the P1 dynamics of an OISL, such as frequency-hopping sequences, nonlinear frequency-modulated (NLFM) microwave waveforms, and dual-chirp LFM waveforms [32]–[34]. Recently, we proposed an MWP radar based on the P1 dynamics of an OISL [35]. However, only a proof-of-concept experiment was conducted, which did not provide a detailed analysis of the transmit signal or prove the flexible tunability of the operating parameters. In addition, fast and high-resolution ISAR imaging capability was not investigated, which is a key function to enhance the performance of target recognition and is highly desired in practical applications of MWP radars.

In this paper, we put forward a novel photonics-based radar with an OISL without the requirement of extra RF sources, where fast and high-resolution imaging, and flexible tunability are realized. In the transmitter, a broadband LFM signal is generated by the controlled P1 oscillation of an OISL. In the receiver, photonic de-chirping and a low-speed ADC are used to realize fast signal processing. In the experimental demonstration, a fully photonics-based inverse synthetic aperture radar (ISAR) system with a bandwidth of 4 GHz is established, where a high range resolution reaching ∼1.88 cm, and a 2D imaging resolution as high as ∼1.88 cm × ∼2.00 cm are achieved with a sampling rate of 100 MSa/s. Additionally, the flexible tunability of the radar is also investigated by adjusting the central frequency, bandwidth, frequency band, and temporal period of the transmitting waveform. To the best of our knowledge, this is the first demonstration of an RF-source-free reconfigurable MWP radar with fast and high-resolution target detection and imaging capability.

II. Experimental Setup and Principle

The schematic diagram of the proposed RF-source-free MWP radar based on an OISL is sketched in Fig. 1(a). In the transmitter, the continuous-wave (CW) light from a master laser (ML) is split into two branches by an 80/20 optical coupler (OC). The optical signal in the lower branch is used as the optical carrier in the receiver. In the upper branch, the optical signal is injected into a slave laser (SL) after passing through a variable optical attenuator (VOA), a dual-drive Mach–Zehnder modulator (DMZM), and an optical circulator (CIR). Here, the VOA is used to achieve a suitable injection strength. Under proper optical injection parameters, i.e., injection strength and frequency detuning between the ML and SL, the injected SL can operate in the desired P1 oscillation state. The spectral characteristics in the P1 state are illustrated in Fig. 1(b) [36]. A single-frequency microwave signal (f_o) can be generated after optical-to-electrical conversion. For a given detuning frequency, the P1 frequency would increase with the injection strength. Therefore, a low-speed control signal $V(t)$ is used to drive the MZM for rapid variation of the optical injection strength. Through properly setting the $V(t)$ to have a near-sawtooth profile, a broadband LFM signal can be generated after the photodetector (PD1). Then, in order to improve the phase-noise performance of the generated LFM signal, a delay-matched optoelectronic feedback loop is built, where half of the LFM signal is separated and fed back to drive DMZM1 and a variable electrical attenuator (VEA) is inserted to optimize the feedback strength. Here, the round-trip time of the feedback loop, which is mainly induced by a section of single-mode fiber (SMF), can be estimated by measuring the free spectral range (FSR) of the optoelectronic feedback cavity in the electrical spectrum analyzer (ESA). After carefully matching the round-trip time with the temporal period of the LFM signal, Fourier domain mode locking (FDML) is successfully established [37], [38]. Afterwards, the performance-enhanced LFM signal is amplified by an electrical amplifier (EA1) before splitting into two parts by an electrical power divider (Div). One part of the LFM signal is used as a reference for de-chirping the radar echoes, and the other part is launched into air through a transmit antenna (Tx) for target detection. It should be noted that a single-drive MZM can also be used in the transmitter to replace DMZM1, and the control signal $V(t)$ can be applied to the bias port of the MZM [38].

In the receiver, the echoes reflected from the targets are collected by a receive antenna (Rx) and properly amplified by another electrical amplifier (EA2). The reference LFM signal

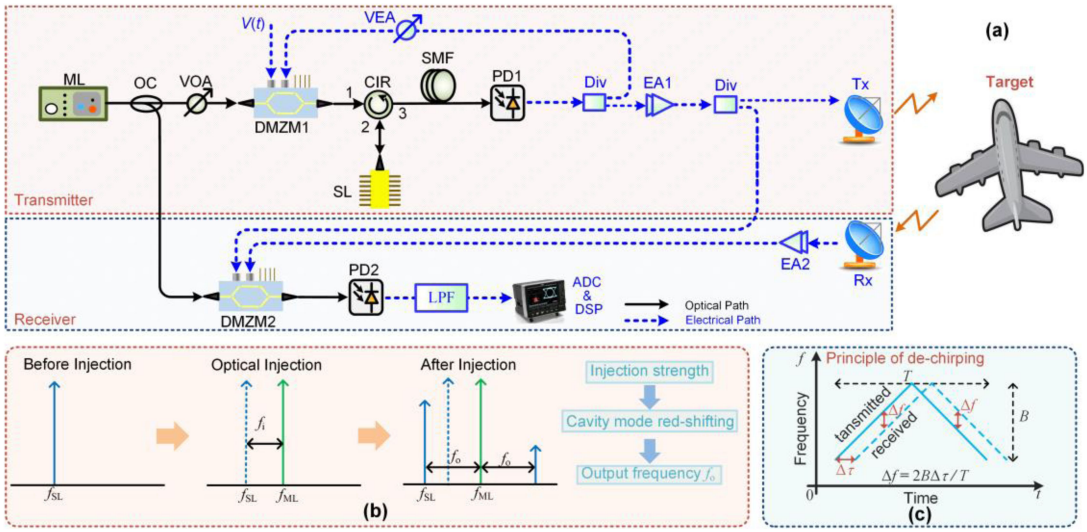

Fig. 1. (a) Schematic diagram of the proposed RF-source-free MWP radar, (b) illustration of spectral characteristic in the P1 state, (c) principle of de-chirping. ML: master laser; OC: optical coupler; VOA: variable optical attenuator; DMZM: dual-drive Mach-Zehnder modulator; CIR: optical circulator; SL: slave laser; SMF: single-mode fiber; PD: photodetector; Div: power divider; VEA: variable electrical attenuator; EA: electrical amplifier; LPF: low pass filter; ADC: analog to digital converter; DSP: digital signal processing; Tx: transmitting antenna; Rx: receiving antenna.

and echoes are separately applied to one of the arms of the DMZM2. The modulated optical signal is then sent to another photodetector (PD2) to perform photonic frequency mixing. After PD2, an electrical low-pass filter (LPF) is employed to remove high-frequency interference and a de-chirped signal is generated. Because of the bandwidth compression property brought by broadband photonic de-chirping, fast and even real-time radar signal processing is feasible. Subsequently, the de-chirped signal can be sampled by a low-speed ADC with a high precision. Then, a simple spectral analysis is performed by a digital signal processor (DSP) to acquire the range information of targets.

The principle for de-chirping of an LFM signal is shown in Fig. 1(c). For the simplest situation of single-target detection, a dual-chirp LFM signal with up- and down-chirp alternatively is adopted, and thus a de-chirped signal with a frequency of $\Delta f = 2B\Delta\tau/T$ will be obtained, where B is the bandwidth, T is the temporal period and $\Delta\tau$ is the time delay. The distance of the target is estimated as

$$L = \frac{\Delta\tau}{2}c = \frac{c}{4B}T\Delta f \tag{1}$$

where c is the velocity of light in vacuum. The minimum spectral spacing that can be distinguished is $\Delta f_{\min} = 1/T$, which results in the range resolution below

$$L_{\mathrm{RES}} = \frac{c}{4B}\ . \tag{2}$$

III. Experimental Results

A. Radar Signal Generation

To verify the feasibility of the proposed RF-source-free MWP radar system based on an OISL, an experiment is performed based on the setup in Fig. 1. A commercial distributed-feedback (DFB) semiconductor laser (Wuhan 69 Inc.) serves as the SL, and its optical spectrum is shown in the orange dot curve in Fig. 2(a), whose free-running frequency (f_{SL}) and optical power are 193.284 THz and 6.5 dBm, respectively. The ML (Newkey Photonics Inc.) operating at a frequency of $f_{\mathrm{ML}} = 193.280$ THz (a detuning of -4 GHz) outputs a CW light, which is injected into the SL with an injection power of -9 dBm, as depicted in the green dashed curve in Fig. 2(a). In this case, the SL outputs a typical single-sideband (SSB) P1 optical spectrum. As presented in the gray solid curve in Fig. 2(a), the sidebands are equally separated by the P1 oscillation frequency $f_{\mathrm{o}} = 16.5$ GHz. Two highly dominant components, i.e., a red-shifted cavity mode and a regenerated optical carrier, are observed to be more than 20 dB stronger than other components. At the output of PD1 (Optilab Inc., 30 GHz), a microwave signal can be generated with a frequency of f_{o}. It has been proven that the microwave frequency f_{o} can be easily controlled by varying the optical injection strength, which can be achieved by tuning the VOA or bias voltage of DMZM1. We measure the relationship between the P1 oscillation frequency and the bias voltage applied to DMZM1 (Fujitsu FTM7937, bandwidth ~25 GHz), as shown in Fig. 2(b). As can be seen, the measured relationship is not ideally linear, which might originate from the nonlinear amplitude transfer function of the injected SL and MZM.

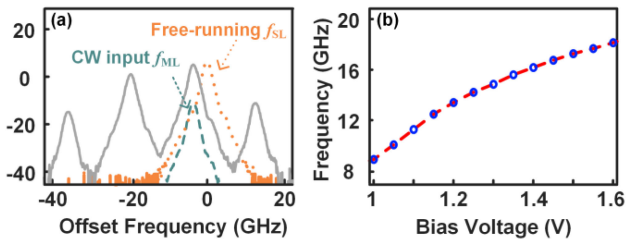

Fig. 2. (a) Optical spectra of the CW input ML (green dashed curve), free-running SL (orange dotted curve), and P1 dynamics (gray solid curve), (b) the relationship between the P1 oscillation frequency and the bias voltage applied to DMZM1.

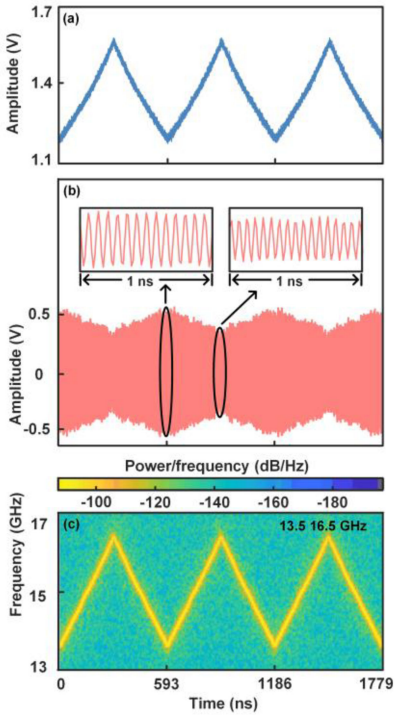

Fig. 3. The results for dual-chirp LFM signal generation. (a) Bias voltage applied to DMZM1, (b) temporal waveforms, and (c) time-frequency characteristics.

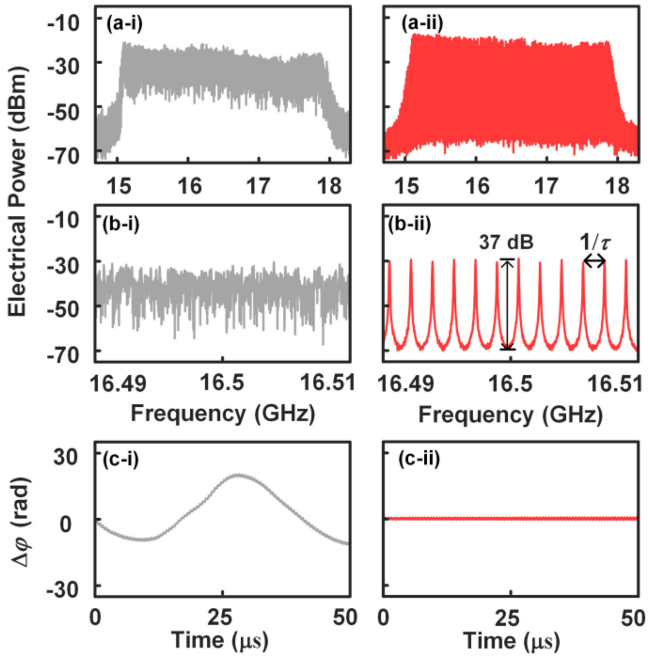

Fig. 4. (a) Electrical spectra, (b) detailed electrical spectra, and (c) phase deviation $\Delta\varphi$ of the generated dual-chirp LFM signal. (i) Without feedback, (ii) with feedback.

In order to generate a desired dual-chirp LFM signal for radar detection, the profile of bias voltage $V(t)$ is designed based on the measured relationship in Fig. 2(b). As plotted in Fig. 3(a), a control signal with an amplitude of 0.32 V and a period of 593 ns is applied to DMZM1. Consequently, a dual-chirp LFM signal is acquired in a 20-GHz oscilloscope (LeCroy 820Zi-B), and its temporal waveform is given in Fig. 3(b). The insets show the detailed waveforms at the minimum and maximum instantaneous frequency of a period, respectively. Fig. 3(c) depicts the instantaneous frequency characteristics of the acquired waveform based on short-time Fourier transform. As can be seen, a dual-chirp LFM is successfully generated with a bandwidth of 3 GHz (from 15 to 18 GHz) and a period of 593 ns. It is worth noting that, the bias drifting of DMZM1 will cause a minor change in the frequency range of the transmit signal. Thus, due to the change of environmental conditions in practical applications, bias stabilization and/or other stabilization methods are required to guarantee the stability of system performance.

For noise reduction, optoelectronic feedback stabilization is adopted by connecting the generated dual-chirp LFM signal to the RF port of the DMZM1, and the electrical feedback power is around −20 dBm. Fig. 4(a) and (b) show the electrical spectra of the generated dual-chirp LFM signals (i) with and (ii) without feedback, which are measured by a 40-GHz ESA (R&S FSV40). When the optoelectronic feedback stabilization is not applied, the generated dual-chirp LFM signal suffers from large phase noise and uncorrelated phase relationship. As shown in Fig. 4(a-i) and (b-i), no obvious comb-like features are observed in its electrical spectra. In contrast, when optoelectronic feedback stabilization is enabled by carefully matching the round-trip time of the feedback loop (τ) to the period of the dual-chirp LFM signal, the Fourier domain mode-locking (FDML) state can be established. Due to the fixed phase relationship and reduced phase noise, a comb-like spectrum with a high signal-to-noise ratio (SNR) is obtained in Fig. 4(a-ii). A zoomed spectrum with a frequency span of 20 MHz is plotted in Fig. 4(b-ii), where sharp comb components separated by $1/\tau$ are observed, and the comb contrast R reaches 37 dB. The effect of feedback stabilization is further verified by calculating the phase deviation $\Delta\varphi$ of the generated dual-chirp LFM signal. Here, the phase deviation $\Delta\varphi$ is calculated by mixing the measured dual-chirp LFM waveform with an ideal one, and the results are plotted in Fig. 4(c) over a long duration of 50 μs. In Fig. 4(c-i), the generated dual-chirp LFM signal has a significant phase deviation fluctuation, indicating its poor phase noise performance without feedback. As for Fig. 4(c-ii), with feedback, the phase deviation fluctuation of the dual-chirp LFM signal is significantly reduced and remains within $\pm\pi/7$ for a duration time of 50 μs. Thus, effective phase noise reduction is achieved through optoelectronic feedback stabilization.

B. De-Chirping of Radar Echoes

Next, the capability of the photonics-based de-chirping in our radar system is evaluated. The stabilized dual-chirp LFM signal (15-18 GHz, 593 ns) is amplified by EA1 (4.5-18.6 GHz, 40 dB) before being sent to the transmit antenna (Tx, 12.4 GHz-18 GHz). A trihedral corner reflector (TCR) made of aluminum acts as a target. An individual receive antenna (Rx, 12.4 GHz-18 GHz) is used to receive the echo. The target is placed 65 cm away from the antenna pair, as presented in Fig. 5(a). After being

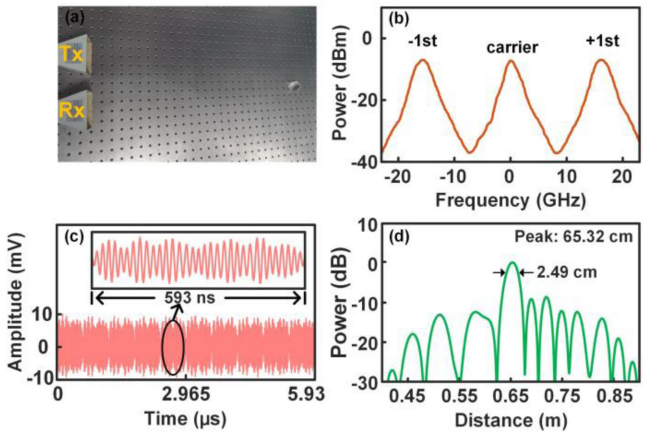

Fig. 5. (a) Configuration for single-target detection, (b) optical spectrum after DMZM2, (c) temporal waveform, and (d) spectrum of the de-chirped signal.

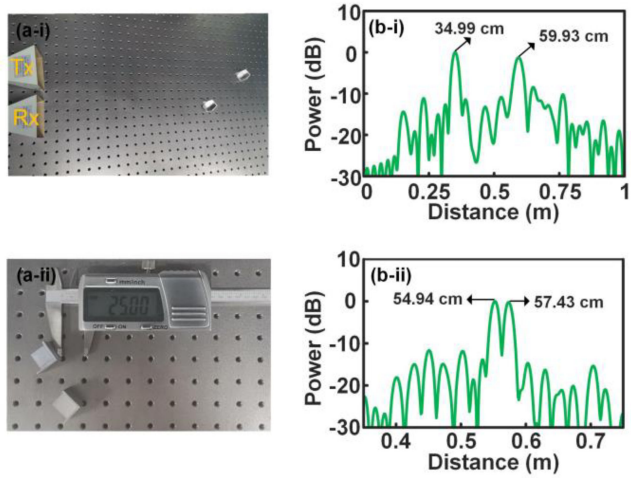

Fig. 6. (a) Configuration for dual-target detection, and (b) normalized electrical spectrum of the de-chirped signal. (i) When two targets are separated by 25 cm, (ii) when two targets are separated by 2.5 cm.

reflected by the target, the echo is first amplified by EA2 (6-18.5 GHz, 28 dB) and then connected to the RF port of DMZM2 (Fujitsu FTM7937) to modulate the optical carrier. The bias voltage of DMZM2 is set at the minimum transmission point (MITP) because it can suppress the optical carrier to reduce the optical power and eliminate the interference of high-order sidebands. The optical spectrum after DMZM2 is shown in Fig. 5(b), where the $\pm$1st-order sidebands contain both the local reference signal and the echo signal. PD2 (Conquer Inc., 10 GHz) is used to detect the frequency difference between the reference signal and the echo signal, and the resultant beating signal passes through an LPF with a bandwidth of 100 MHz to obtain the de-chirped signal. The de-chirped signal is then captured by an electrical ADC with a sampling rate of 500 MSa/s. Fig. 5(c) shows the captured waveform of the de-chirped signal in ten periods, and a detailed waveform of one period is shown in the inset. Based on Equation (1), the electrical spectrum of the de-chirped signal is obtained by performing a fast Fourier transform (FFT) on the captured waveforms. From Fig. 5(d), a dominant spectral peak at 65.32 cm is observed, indicating that a small measurement error of only 3.2 mm is achieved.

Then, a dual-target detection experiment is performed, and the system configuration is illustrated in Fig. 6(a-i), where two metal targets are placed side by side but separated by a distance of ΔD along the range direction. Fig. 6(b-i) is the power spectrum of the de-chirped signal when the two targets are 35 cm and 60 cm away from the antenna pair, respectively. The two peaks are located at 34.99 cm and 59.93 cm, and the calculated distance ΔD is 24.94 cm. In Fig. 6(a-ii), the distance between the two targets is reduced to 2.5 cm, which is equal to the theoretical range resolution, and two spectral peaks with a spacing of 2.49 cm are still observed in Fig. 6(b-ii). This implies that these two targets can be easily distinguished.

C. Ultra-Flexible Tunability

Multifunction adaptive radars with frequency agility and other reconfigurable operating parameters are highly desired in future radar applications. Since the proposed RF-source-free radar

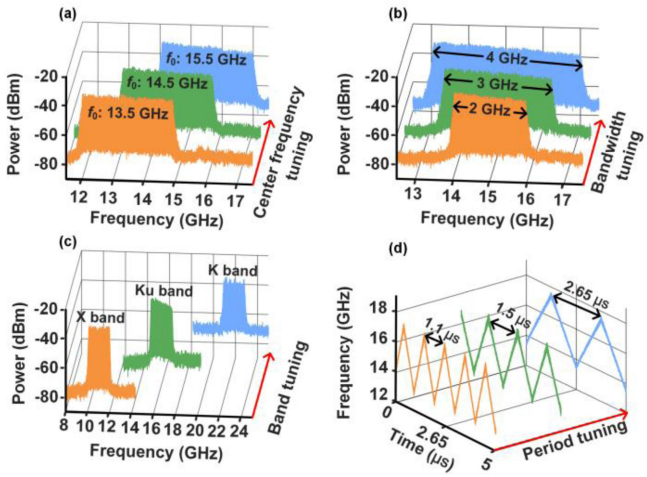

Fig. 7. Reconfigurability of the transmitting waveform. (a) The center frequency is tuned from 13.5 GHz to 15.5 GHz, (b) the bandwidth is tuned from 2 GHz to 4 GHz, (c) the frequency band is tuned from the X band to the Ku band, and (d) the temporal period is tuned from 1.1 μs to 2.65 μs.

has eliminated the frequency limitation imposed by external RF sources, it can be easily reconfigured to other operating parameters. As shown in Fig. 7, the flexible tunability of the radar is also investigated by adjusting the central frequency, bandwidth, frequency band, and temporal period of the transmitting waveform. For central frequency tuning, the injection power of the ML is carefully tuned while other parameters remain constant. As can be seen in Fig. 7(a), the central frequency of the electrical spectra is tuned to 13.5 GHz, 14.5 GHz, and 15.5 GHz in a bandwidth of 3 GHz by changing the optical injection power from -12 dBm, to -11 dBm, and -10 dBm. For bandwidth tuning, the amplitude of bias voltage $V(t)$ applied to DMZM1 is tuned while other parameters remain fixed. Fig. 7(b) shows the electrical spectra of the generated dual-chirp LFM signals with different bandwidths, where the bandwidth of 2 GHz, 3 GHz, and 4 GHz corresponds to the amplitude of 0.22 V, 0.32 V, and 0.4 V, respectively. The capability of operating in different

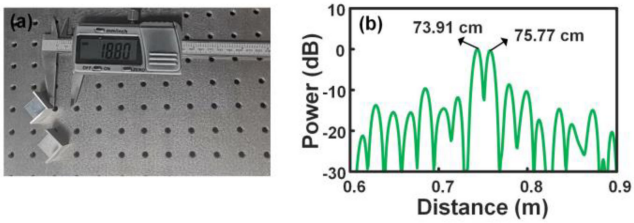

Fig. 8. (a) Configuration for ranging resolution measurement, (b) spectrum of the de-chirped signal when two targets are separated by 1.88 cm.

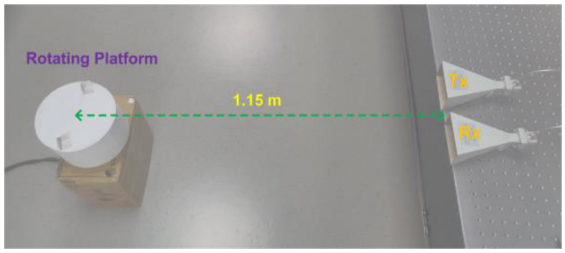

Fig. 9. Photograph of the experimental setup including an antenna pair and a rotating platform.

frequency bands is demonstrated in Fig. 7(c). By setting the master-slave detuning frequency to −8 GHz, −4 GHz, and 15 GHz, respectively, the dual-chirp LFM signal is successfully generated in the X, Ku, and K bands. In addition, tuning of the temporal period is realized by adjusting the period of $V(t)$ and matching the round-trip time of the feedback loop with different lengths of SMF. As can be seen in Fig. 7(d), the time-frequency curves of the generated dual-chirp LFM signals (13.5-17.5 GHz) with a period of 1.1 μs, 1.5 μs, and 2.65 μs are respectively plotted based on Hilbert transform. It should be noted that the central frequency and bandwidth of the dual-chirp LFM signal by the developed radar transmitter can be further increased if a PD with a larger bandwidth is available.

D. ISAR Imaging Ability

Finally, a proof-of-concept microwave ISAR imaging experiment is conducted, where the proposed MWP radar operates in the Ku band with a bandwidth of 4 GHz (13-17 GHz) and a temporal period of 2.65 μs. As shown in Fig. 8(a), the ranging resolution is analyzed by performing a dual-target detection experiment when the two targets are placed side by side but separated by a distance of 1.88 cm along the range direction. After a 100 MSa/s ADC and DSP, the result of photonics-based de-chirping is plotted in Fig. 8(b), where two dominant peaks are located at 73.91 cm and 75.77 cm, resulting in a calculated distance of 1.86 cm. The calculated result is very close to the actual value, indicating that the range resolution reaches ∼1.88 cm due to the increased bandwidth of 4 GHz.

Fig. 9 is a photograph of the experimental setup of ISAR imaging including an antenna pair and a rotating platform. The rotating platform is placed at a distance of 115 cm away from the antenna pair, and is set to have a rotation speed of 900° per second. Here, the target distance is restricted by both the limited indoor space of our laboratory and the small transmit

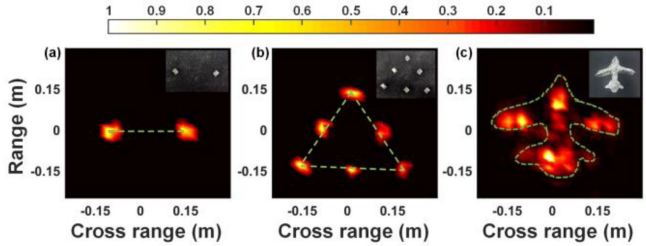

Fig. 10. ISAR images of (a) two targets, (b) multiple targets, and (c) an airplane model.

power. By using a high-power amplifier in the transmitter, the detection range of the proposed MWP radar in the field trial can be effectively increased to hundreds or even thousands of meters [39], [40]. The cross-range resolution of ISAR imaging is given by [9]

$$C_{\mathrm{RES}} = \frac{c}{2\theta f_{\mathrm{c}}} \tag{3}$$

where f_{c} is the center frequency of the dual-chirp LFM signal, θ is the angle of target rotating during the coherent integration time.

Fig. 10 shows the ISAR image results, in which the pictures of the actual object are illustrated as the insets. The ISAR images are constructed by executing a Range-Doppler (RD) algorithm on the de-chirped signal in an integration time of 31.8 ms. The corresponding ISAR viewing angle θ and cross-range resolution C_{RES} are 0.5 rad and ∼2.00 cm, respectively. According to Fig. 8, the range resolution reaches ∼1.88 cm, leading to a 2D imaging resolution as high as ∼1.88 cm × ∼2.00 cm. Here, the integration time should be scaled to a larger value for achieving the same cross-range resolution at a lower rotation speed in practical applications. For instance, in the ISAR imaging experiment of a non-cooperative UAV, an integration time of 160 ms is used [39].

Fig. 10(a)-(c) show the constructed ISAR images. Firstly, two targets are placed on the rotating platform with a cross-range distance of 30 cm. Fig. 10(a) shows the corresponding imaging results, in which the two targets can be clearly distinguished, and the measured distance agrees well with the real value. Secondly, ISAR imaging of multiple targets like an equilateral triangle constitute by six TCRs is performed. The results in Fig. 10(b) confirm the high resolution of the proposed MWP radar based on an OISL. Finally, the ISAR imaging of an airplane model (size: 30 cm × 30 cm) is also obtained, as shown in Fig. 10(c), which again clearly proves that a high-resolution imaging radar is accomplished.

IV. Discussions and Conclusion

Commercially available mm-wave electronics radars for autonomous driving usually operate at approximately 60-77 GHz with a maximum bandwidth of 4 GHz [41]. Due to the use of multiple stages of frequency conversion, the signal purity and the frequency agility of the radar transmit signals would be limited. Moreover, it is difficult to further enhance the operating bandwidth, which has been proven to be a critical parameter to

improve the accuracy of target recognition in radar systems. As a comparison, the generation of radar signals with a bandwidth of more than 8 GHz is feasible based on the MWP approaches, which can support a higher resolution for target detection and recognition [42].

In this paper, we proposed and experimentally demonstrated a novel RF-source-free reconfigurable MWP radar, that is capable of optically generating and processing broadband LFM microwave signals without using any RF sources. To the best of our knowledge, this is the first demonstration of an RF-source-free MWP radar with fast and high-resolution target detection and imaging capability. Compared with existing schemes based on microwave photonic frequency multiplication, the proposed MWP radar has eliminated the requirements of an IF-LFM signal by adding a slave laser, resulting in a reduced equipment complexity/cost as well as a potential of photonic integration [43], [44]. In addition, without the limitation of external RF sources, our approach also has an ultra-flexible tunability in that the main operating parameters of radar are adjustable.

In the experiment, a fully photonics-based radar with a bandwidth of 4 GHz (13-17 GHz, 2.65 μs) is established for fast, high-resolution detection and ISAR imaging. The results show that a high range resolution reaching 1.88 cm and a 2D imaging resolution as high as $\sim$1.88 cm $\times$ $\sim$2.00 cm are achieved with a sampling rate of 100 MSa/s in the receiver. Besides, the flexible tunability of the radar is also confirmed by adjusting the central frequency, bandwidth, frequency band, and temporal period of the transmitting waveform. Thanks to the broadly tunable P1 oscillation frequency of an OISL, the central frequency and bandwidth of the developed radar scheme can be further increased, if PDs, antennas, and electrical amplifiers with a larger bandwidth are available. The proposed radar scheme features low cost, a simple structure, and high reconfigurability, which, hopefully, is to be used in future multifunction adaptive and miniaturized radars.

REFERENCES

[1] M. I. Skolnik, *Radar Handbook*, 3rd ed. New York, NY, USA: McGraw-Hill, 2008.

[2] B. B. Cheng *et al.*, "Real-time imaging with a 140 GHz inverse synthetic aperture radar," *IEEE Trans. THz Sci. Technol.*, vol. 3, no. 5, pp. 606–616, Sep. 2013.

[3] S. Pan and Y. Zhang, "Microwave photonic radars," *J. Lightw. Technol.*, vol. 38, no. 19, pp. 5450–5484, Oct. 2020.

[4] J. D. McKinney, "Photonics illuminates the future of radar," *Nature*, vol. 507, no. 7492, pp. 310–314, Mar. 2014.

[5] P. Ghelfi *et al.*, "A fully photonics-based coherent radar system," *Nature*, vol. 507, no. 7492, pp. 341–345, Mar. 2014.

[6] N. Qian, W. Zou, S. Zhang, and J. Chen, "Signal-to-noise ratio improvement of photonic time-stretch coherent radar enabling high-sensitivity ultrabroad W-band operation," *Opt. Lett.*, vol. 43, no. 23, pp. 5869–5872, Dec. 2018.

[7] S. Peng *et al.*, "High-resolution W-band ISAR imaging system utilizing a logic-operation-based photonic digital-to-analog converter," *Opt. Express*, vol. 26, no. 2, pp. 1978–1987, Jan. 2018.

[8] R. Li *et al.*, "Demonstration of a microwave photonic synthetic aperture radar based on photonic-assisted signal generation and stretch processing," *Opt. Express*, vol. 25, no. 13, pp. 14334–14340, Jun. 2017.

[9] F. Zhang *et al.*, "Photonics-based broadband radar for high-resolution and real-time inverse synthetic aperture imaging," *Opt. Express*, vol. 25, no. 14, pp. 16274–16281, Jul. 2017.

[10] A. Wang *et al.*, "Ka-band microwave photonic ultra-wideband imaging radar for capturing quantitative target information," *Opt. Express*, vol. 26, no. 16, pp. 20708–20717, Aug. 2018.

[11] S. Li *et al.*, "Chip-based microwave-photonic radar for high resolution imaging," *Laser Photon. Rev,* vol. 14, no. 10, Aug. 2020, Art. no. 1900239.

[12] X. Ye, F. Zhang, Y. Yang, and S. Pan, "Photonics-based radar with balanced I/Q de-chirping for interference-suppressed high-resolution detection and imaging," *Photon. Res,* vol. 7, no. 3, pp. 265–272, Mar. 2019.

[13] F. Zhang, B. Gao, and S. Pan, "Photonics-based MIMO radar with high-resolution and fast detection capability," *Opt. Express*, vol. 26, no. 13, pp. 17529–17540, Jun. 2018.

[14] F. Scotti, S. Maresca, L. Lembo, G. Serafino, A. Bogoni, and P. Ghelfi, "Widely distributed photonics-based dual-band MIMO radar for harbour surveillance," *IEEE Photon. Technol. Lett.*, vol. 32, no. 17, pp. 1081–1084, Sep. 2020.

[15] P. Ghelfi, F. Laghezza, F. Scotti, D. Onori, and A. Bogoni, "Photonics for radars operating on multiple coherent bands," *J. Lightw. Technol.*, vol. 34, no. 2, pp. 500–507, Jan. 2016.

[16] J. Cao *et al.*, "Photonic deramp receiver for dual-band LFM-CW radar," *J. Lightw. Technol.*, vol. 37, no. 10, pp. 2403–2408, May 2019.

[17] B. Gao, F. Zhang, E. Zhao, D. Zhang, and S. Pan, "High-resolution phased array radar imaging by photonics-based broadband digital beamforming," *Opt. Express*, vol. 27, no. 9, pp. 13194–13203, Apr. 2019.

[18] A. Wang *et al.*, "Microwave photonic radar system with ultra-flexible frequency-domain tunability," *Opt. Express*, vol. 29, no. 9, pp. 13887–13898, Apr. 2021.

[19] X. Zhang, H. Zeng, J. Yang, Z. Yin, Q. Sun, and W. Li, "Novel RF-source-free recon urable microwave photonic radar," *Opt. Express*, vol. 28, no. 9, pp. 13650–136618, Apr. 2020.

[20] X. Q. Qi and J. M. Liu, "Photonic microwave applications of the dynamics of semiconductor lasers," *IEEE J. Sel. Topics Quantum Electron.*, vol. 17, no. 5, pp. 1198–1211, Sep./Oct. 2011.

[21] S. C. Chan, S. K. Hwang, and J. M. Liu, "Radio-over-fiber AM-to-FM upconversion using an optically injected semiconductor laser," *Opt. Lett.*, vol. 31, no. 15, pp. 2254–2256, Aug. 2006.

[22] S. C. Chan and J. M. Liu, "Tunable narrow-linewidth photonic microwave generation using semiconductor laser dynamics," *IEEE J. Sel. Topics Quantum Electron.*, vol. 10, no. 5, pp. 1025–1032, Sep. 2004.

[23] Y. H. Hung and S. K. Hwang, "Photonic microwave stabilization for period-one nonlinear dynamics of semiconductor lasers using optical modulation sideband injection locking," *Opt. Express*, vol. 23, no. 5, pp. 6520–6532, Mar. 2015.

[24] J. S. Suelzer, T. B. Simpson, P. Devgan, and N. G. Usechak, "Tunable, low-phase-noise microwave signals from an optically injected semiconductor laser with opto-electronic feedback," *Opt. Lett.*, vol. 42, no. 16, pp. 3181–3184, Aug. 2017.

[25] P. Zhou, F. Z. Zhang, D. C. Zhang, and S. L. Pan, "Performance enhancement of an optically-injected-semiconductor-laser-based optoelectronic oscillator by subharmonic microwave modulation," *Opt. Lett.*, vol. 43, no. 21, pp. 5439–5442, Nov. 2018.

[26] Y. Li, L. Fan, G. Xia, and Z. Wu, "Tunable and broadband microwave frequency comb generation using optically injected semiconductor laser nonlinear dynamics," *IEEE Photon. J,* vol. 9, no. 5, Jul. 2017, Art. no. 1900239.

[27] H. Zhu, R. Wang, T. Pu, P. Xiang, J. Zheng, and T. Fang, "A novel approach for generating flat optical frequency comb based on externally injected gain-switching distributed feedback semiconductor laser," *Laser Phys. Lett.*, vol. 14, no. 2, Feb. 2017, Art. no. 02601.

[28] Y. Doumbia, T. Malica, D. Wolfersberger, K. Panajotov, and M. Sciamanna, "Nonlinear dynamics of a laser diode with an injection of an optical frequency comb," *Opt. Express*, vol. 28, no. 21, pp. 30379–30390, Oct. 2020.

[29] P. Zhou, F. Zhang, B. Gao, and S. Pan, "Optical pulse generation by an optoelectronic oscillator with optically injected semiconductor laser," *IEEE Photon. Technol. Lett.*, vol. 28, no. 17, pp. 1827–1830, Sep. 2016.

[30] P. Zhou, F. Zhang, Q. Guo, and S. Pan, "A modulator-free photonic triangular pulse generator based on semiconductor lasers," *IEEE Photon. Technol. Lett.*, vol. 30, no. 14, pp. 1317–13204, Jul. 2018.

[31] P. Zhou, F. Zhang, Q. Guo, and S. Pan, "Linearly chirped microwave waveform generation with large time-bandwidth product by optically injected semiconductor laser," *Opt. Express*, vol. 24, no. 16, pp. 18460–18467, Aug. 2016.

[32] P. Zhou, F. Z. Zhang, X. W. Ye, Q. S. Guo, and S. L. Pan, "Flexible frequency-hopping microwave generation by dynamic control of optically injected semiconductor laser," *IEEE Photon. J.*, vol. 8, no. 6, pp. 5501909–5501909, Dec. 2016.

[33] P. Zhou *et al.*, "Generation of NLFM microwave waveforms based on controlled period-one dynamics of semiconductor lasers," *Opt. Express*, vol. 28, no.no. 22, pp. 32647–32656, Oct. 2020.
[34] P. Zhou, H. Chen, N. Li, R. Zhang, and S. Pan, "Photonic generation of tunable dual-chirp microwave waveforms using a dual-beam optically injected semiconductor laser," *Opt. Lett.*, vol. 45, no. 6, pp. 1342–1345, Mar. 2020.
[35] P. Zhou, R. H. Zhang, Z. D. Jiang, N. Q. Li, and S. L. Pan, "Demonstration of a RF-source-free microwave photonic radar based on an optically injected semiconductor laser," in *Proc. Opt. Fiber Commun. Conf. Expo.*, 2021, pp. 1–3.
[36] S. K. Hwang, J. M. Liu, and J. K. White, "Characteristics of period-one oscillations in semiconductor lasers subject to optical injection," *IEEE J. Sel. Top. Quantum Electron.*, vol. 10, no. 5, pp. 974–981, Sep. 2004.
[37] T. Hao *et al.*, "Breaking the limitation of mode building time in an optoelectronic oscillator," *Nature Commun.*, vol. 9, no. 1, May. 2018, Art. no. 1839.
[38] J. P. Zhuang, X. Z. Li, S. S. Li, and S. C. Chan, "Frequency-modulated microwave generation with feedback stabilization using an optically injected semiconductor laser," *Opt. Lett.*, vol. 41, no. 24, pp. 5764–5767, Dec. 2016.
[39] F. Zhang *et al.*, "Photonics-based real-time and high resolution ISAR imaging of non-cooperative target," *Chin. Opt. Lett.*, vol. 15, no. 11, Nov. 2017, Art. no. 112801.
[40] R. Li *et al.*, "Demonstration of a microwave photonic synthetic aperture radar based on photonic assisted signal generation and stretch processing," *Opt. Express*, vol. 25, no. 13, pp. 14334–14340, Jun. 2017.
[41] *AWR1843AOP Single-Chip 77- and 79-GHz FMCW Radar Sensor*, Dallas, Texas, USA: Texas Instruments, Accessed: Dec. 25, 2021. [Online]. Available: https://www.ti.com/lit/ds/symlink/awr1843aop.pdf?ts=1634713647318&ref_url=https%253A%252F%252Fwww.ti.com%252F
[42] J. Li, F. Zhang, Y. Xiang, and S. Pan, "Towards small target recognition with photonics-based high resolution radar range profiles," *Opt. Express*, vol. 29, no. 20, pp. 31574–31581, Sep. 2021.
[43] L. Guo *et al.*, "Linearly chirped microwave generation using a monolithic integrated amplified feedback laser," *IEEE Photon. Technol. Lett.*, vol. 29, no. 21, pp. 1915–1918, Nov. 2017.
[44] J. Li *et al.*, "Photonic generation of linearly chirped microwave waveforms using a monolithic integrated three-section laser," *Opt. Express*, vol. 26, no. 8, pp. 9676–9685, Apr. 2018.

Pei Zhou (Member, IEEE) received the B.S. and Ph.D. degrees from the Nanjing University of Aeronautics and Astronautics (NUAA), Nanjing, China, in 2013 and 2019, respectively. From 2017 to 2018, he was a Visiting Scholar with the University of California, Los Angeles, CA, USA. He is currently with the School of Optoelectronic Science and Engineering, Soochow University, Suzhou, China. His main research interests include microwave photonics, nonlinear laser dynamics, and optical chaos.

Renheng Zhang received the B.S. degree in optoelectronics from the Qilu University of Technology, Jinan, China, in 2019. He is currently working toward the M.S. degree with Soochow University, Suzhou, China. His main research interests include nonlinear laser dynamics and microwave photonic signal generation.

Nianqiang Li (Member, IEEE) received the B.S. degree in communication engineering and the Ph.D. degree in optoelectronics from Southwest Jiaotong University, Chengdu, China, in 2008 and 2016, respectively. His thesis work concerned nonlinear dynamics of semiconductor lasers and its applications to secure communications and random number generation. From 2013 to 2014, he was a Visiting Scholar with the Georgia Institute of Technology (Georgia Tech), Atlanta, GA, USA. From 2016 to 2018, he was with the School of Computer Science and Electronic Engineering, University of Essex, Colchester, U.K., as a Postdoctoral Researcher focusing on a collaborative EPSRC funded project in U.K. From May 2018 to December 2018, he was with the School of Electrical Engineering and Computer Science, University of Ottawa, Ottawa, ON, Canada, working on microwave photonics. Since January 2019, he has been working with Soochow University, Suzhou, China, as a Full Professor. He is currently with the School of Optoelectronic Science and Engineering, Soochow University. He has authored or coauthored more than 70 peer reviewed journal papers. His current research interests mainly include the area of the laser dynamics, chaos-based communication and random number generation, and microwave photonics. He is an Associate Editor for the IEEE ACCESS.

Zhidong Jiang received the B.S. degree in optoelectronics from Nanjing Tech University, Nanjing, China, in 2020. He is currently working toward the M.S. degree with Soochow University, Suzhou, China. His main research interests include photonics-based microwave signal generation and measurement.

Shilong Pan (Senior Member, IEEE) received the B.S. and Ph.D. degrees in electronic engineering from Tsinghua University, Beijing, China, in 2004 and 2008, respectively. From 2008 to 2010, he was a Vision 2010 Postdoctoral Research Fellow with the Microwave Photonics Research Laboratory, University of Ottawa, Ottawa, ON, Canada. In 2010, he joined the College of Electronic and Information Engineering, Nanjing University of Aeronautics and Astronautics, China, where he is currently a Full Professor and the Executive Director of the Key Laboratory of Radar Imaging and Microwave Photonics, Ministry of Education. He has authored or coauthored more than 400 research papers, including more than 200 articles in peer-reviewed journals and 200 papers in conference proceedings. His research interests include microwave photonics, which include optical generation and processing of microwave signals, analog photonic links, photonics microwave measurement, and integrated microwave photonics.

Prof. Pan is currently an Associate Editor for *Electronics Letters*, the Topical Editor of *Chinese Optics Letters*, and is a Technical Committee Member of IEEE MTT- 22 Microwave Photonics. He was the Chair of a number of international conferences, symposia, and workshops, including the TPC Chair of the International Conference on Optical Communications and Networks in 2015, and TPC Co-Chair of the IEEE International Topical Meeting on Microwave Photonics in 2017. He is a Fellow of OSA, SPIE, and IET. He was selected as an IEEE Photonics Society Distinguished Lecturer in 2019 and 2020.